RSC Advances

PAPER

View Article Online
View Journal | View Issue

Cite this: *RSC Adv.*, 2019, **9**, 18459

Systematic study of the substitution effect on the tetrel bond between 1,4-diazabicyclo[2.2.2]octane and TH_3X†

Mingchang Hou,[a] Kunyu Jin,[a] Qingzhong Li *[a] and Shufeng Liu [b]

Received 5th May 2019
Accepted 3rd June 2019

DOI: 10.1039/c9ra03351c

rsc.li/rsc-advances

A tetrel bond was characterized in the complexes of 1,4-diazabicyclo[2.2.2]octane (DABCO) with TH_3X (T = C, Si, Ge; X= –Me, –H, –OH, $–NH_2$, –F, –Cl, –Br, –I, –CN, $–NO_2$). DABCO engages in a weak tetrel bond with CH_3X but a stronger one with SiH_3X and GeH_3X. SiH_3X is favorable to bind with DABCO relative to GeH_3X, inconsistent with the magnitude of the σ-hole on the tetrel atom. The methyl group in the tetrel donor weakens the tetrel bond but an enhancing effect is found for the other substituents, particularly $–NO_2$. The substitution effect is also related to the nature of the tetrel atom. The halogen substitution from F to I has a weakening effect in the CH_3X complex but an enhancing effect in the SiH_3X complex and a negligible effect in the GeH_3X complex. The above abnormal results found in these complexes can be partly attributed to the charge transfer from the lone pair on the nitrogen atom of DABCO into the anti-bonding orbital σ*(T–X) of TH_3X. The stability of both SiH_3X and GeH_3X complexes is primarily controlled by electrostatic interactions and polarization.

1. Introduction

For a long time, non-covalent interactions have attracted widespread interest because of their important roles in crystal engineering,[1–3] chemical reactions[4–6] and biological systems.[7–9] Hydrogen bonding is one of the most important interactions and other types of interactions have also been proposed.[10–12] Now these interactions are uniformly classified as σ-hole/π-hole interactions. The σ-hole refers to a region with positive electrostatic potentials along a covalent bond end[13] and the π-hole is an area with positive electrostatic potentials perpendicular to a molecular plane.[14] These interactions are also called halogen bond,[15] chalcogen bond,[16] pnicogen bond,[17] and tetrel bond[18] in view of the origin of these σ-holes/π-holes. These σ-holes/π-holes have an attractive interaction with electron donors such as neutral molecules with a lone pair,[19–21] anions,[22] radicals,[23] metal hydrides,[24,25] and π-molecules.[26] Tetrel bonding is an attractive interaction between a group IV atom and an electron donor.[18] This interaction had been explored before the name tetrel bond was proposed.[27–29] For instance, Mitzel *et al.* reported Si···N interactions in the solid-state structure of $Si(ONMe_2)_4$ and related compounds[27,28] and Si···halide contacts were described in perhalocyclohexasilane complexes.[29]

The strength of tetrel bonding primarily determines its properties and applications since most chemical and biochemical processes are mainly accomplished by means of combination of various noncovalent interactions.[30–32] Therefore, more attention was paid to the factors associated with the strength of tetrel bonding. In most cases, tetrel bonding is stronger for the heavier tetrel atom due to its smaller electronegativity and larger polarization. The magnitude of the σ-hole on the tetrel atom enlarges if this atom adjoins with electron-withdrawing atoms or groups, resulting in a stronger tetrel bond. This confirms the conclusion that most of tetrel bonds are dominated by electrostatic interaction.[23] However, the bigger σ-hole may not bring out a stronger tetrel bond in some special circumstances. For instance, when N-heterocyclic carbene (NHC) acts as an electron donor, carbene tetrel bond is stronger for the Si compounds than for the Ge analogues although the latter has the bigger σ-hole.[33] This shows that the dependence of tetrel bonding strength on the magnitude of σ-hole is also related to the nature of electron donor. If the electron donor is strong enough, the strength of tetrel bond is not solely determined by electrostatic and other contributions such as polarization are also important.

Substituents are also an effective method for regulating the strength of non-covalent interactions.[34–43] 6-OCF_3-fulvene is favorable to engage in a weak H-bond with NH_3 but a tetrel bond is formed when the four H atoms in 6-OCF_3-fulvene are replaced by CN groups.[34] The similar change was also reported for the proton effect on the interaction type between pyridine CF_3/furan

[a]*The Laboratory of Theoretical and Computational Chemistry, School of Chemistry and Chemical Engineering, Yantai University, Yantai 264005, People's Republic of China. E-mail: liqingzhong1990@sina.com*

[b]*Shandong Key Laboratory of Biochemical Analysis, College of Chemistry and Molecular Engineering, Qingdao University of Science and Technology, Qingdao 266042, PR China*

† Electronic supplementary information (ESI) available. See DOI: 10.1039/c9ra03351c

CF_3 and NH_3.[44] For the tetrel-bonded complexes of formamidine with TH_3F, electron-donating substituents in formamidine lead to the opposite effect on the strength of the tetrel bond: a weakening effect for –OH and $-OCH_3$ but an enhancement for $-CH_3$ and $-NH_2$.[41] The F substitution in TH_4 (T = C–Sn) has an enhancing effect on the strength of tetrel bonding whether the H opposite to the electron donor or the three peripheral H atoms is replaced.[42] Perfluorinated substitution TF_4 yields the strongest tetrel bonding.[42] The methyl substitution shows a reverse effect on the strength of tetrel bond to the F analogue.[43] TX_3^+ (T = C, Ge, Sn, Pb; X = H, F, Cl, Br) can bind with carbon monoxide and noble gas (Ng) atoms, and the nature of T-CO and T-Ng bonds is also affected by the halogen substitution.[45–47] A question occurs: does the substitution in the tetrel donor on the strength of tetrel bonding depend on the electron-donating ability of an electron donor?

1,4-Diazabicyclo[2.2.2]octane (DABCO) was often used as an organic base in organic syntheses because of its less sterically hindered nitrogen atoms. Using DABCO not only increases the yield of the Morita–Baylis–Hillman (MBH) reaction but also shows very pronounced regioselectivity.[48,49] Importantly, the MBH reaction of benzaldehyde with acrylamide under DABCO catalysis can be carried out in an aqueous system.[50] In addition, as a good linker, DABCO can also form structurally stable complexes with a variety of organic and organometallic compounds.[51] Similarly, there are some studies on the non-covalent interactions such as hydrogen and halogen bonds involved with DABCO.[52–57] A new supramolecular fluorine organic catalyst was prepared by halogen bonding between perfluorooctyl iodide and DABCO, which effectively promoted Baylis–Hillman reaction.[53] DABCO participates in a stronger halogen bond than other neutral bases, indicating that DABCO is a good electron donor.[57]

In this paper, we selected DABCO (Fig. 1) as the electron donor to bind with TH_3X (T = C, Si, Ge; X= –Me, –H, –OH, $-NH_2$, –F, –Cl, –Br, –I, –CN, $-NO_2$). The following questions are answered. How to predict and characterize the tetrel bond between both molecules? Is the strength of tetrel bond consistent with the magnitude of σ-hole on the tetrel atom? How the substituents affect the strength of tetrel bond? Does this substitution effect depend on the nature of the tetrel atom? These tetrel-bonded complexes were studied in view of geometries, energetics, frequencies, charge transfer, orbital interaction, topological analysis and energy decomposition.

2. Methods

All calculations were performed using the Gaussian 09 software.[58] First, the geometries of the complexes and monomers were optimized with the aug-cc-pVDZ basis set using the second-order Møller–Plesset perturbation theory (MP2) method. And then their frequencies were calculated at the same level to affirm that the optimized structures are minima on the potential energy surface and to analyze the frequency shifts. The interaction energy was calculated as difference between the energy of complex and the energies of monomers with their geometries in the complex, and this quantity was corrected for zero-point energy (ZPE) and basis set superposition error (BSSE) using the Boys and Bernardi method.[59]

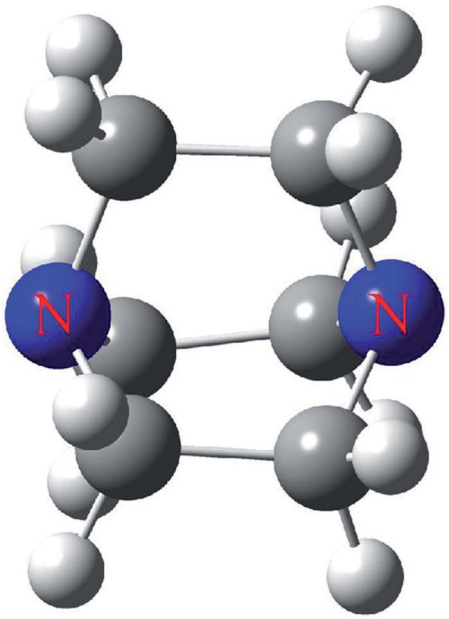

Fig. 1 The structure of DABCO.

The electrostatic potentials of monomers were calculated on the 0.001 au isodensity using the Wave Function Analysis–Surface Analysis Suite (WFA-SAS) program.[60] The AIM2000 package[61] was used to assess the topological parameters at bond critical point (BCP) including electron density, its Laplacian, and energy density. Using the nature bond orbital (NBO) program,[62] charge transfer and orbital interactions were obtained. In order to reveal the nature of the interaction, the GAMESS program[63] was used to decompose the interaction energy into five terms with physical meaning at the MP2/aug-cc-pVDZ level using the Localized Molecular Orbital-Energy Decomposition Analysis (LMOEDA) method.[64]

3. Results and discussion

3.1. MEPs of monomers

Fig. 2 represents the MEP maps of DABCO and three representative molecules of TH_3X. First, there is a blue region (negative MEPs) on either side of the DABCO molecule, corresponding to the lone pair on the two nitrogen atoms in this molecule. And the most negative MEP on the two N atoms is the same with a value of -35.4 kcal mol^{-1}. Then, let's have a look at TH_3X. Considering the similarity for the MEP maps of TH_3X with different X groups, we only plotted the MEP map of SiH_3F, CH_3Me and CH_4 in Fig. 2. A σ-hole (red area) with positive MEPs is found at the X–T bond end in TH_3X excluding CH_3Me and CH_4. In the latter two molecules, the central carbon atom is surrounded by negative MEPs. Therefore, both CH_4 and CH_3Me cannot form a tetrel bond with Lewis bases.

Table 1 lists the extreme value of the electrostatic potential at the end of the X–T bond, which is arranged in an increasing

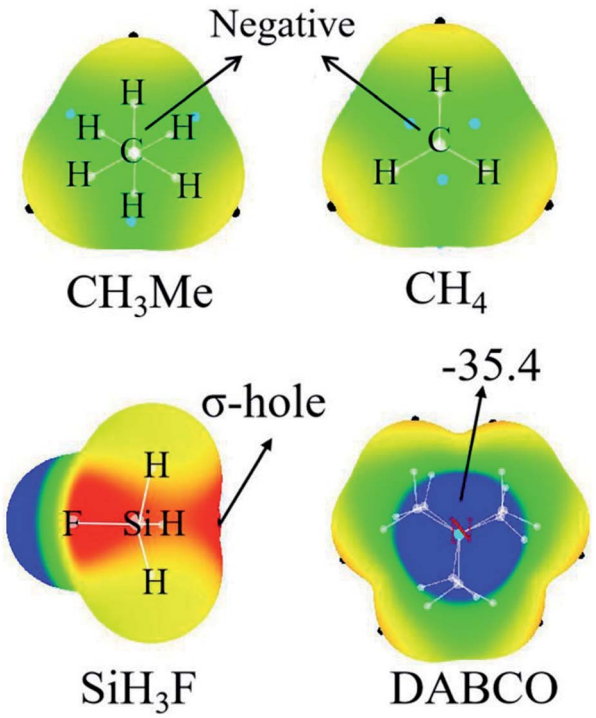

Fig. 2 MEP maps of DABCO, SiH_3F, CH_4 and CH_3Me. Color ranges are: red, greater than 12.5; yellow, between 12.5 and 0; green, between 0 and −12.5; blue, less than −12.5. All quantities are in kcal mol^{-1}.

sequence. When X is hold, the σ-hole enlarges from CH_3X to SiH_3X to GeH_3X due to the smaller electronegativity and larger polarization. The methyl substituent results in a smaller σ-hole for T = Si and Ge or a more negative MEP on the C atom. This means that the methyl group in the tetrel donor is electron-donating. This electron-donating role of methyl group is also related to the nature of the tetrel atom and its effect is largest in SiH_3Me. When X = NH_2 and OH, the σ-hole is enlarged since the N/O atom has greater electronegativity than the tetrel atom and the larger enlargement is found for the –OH group with the similar reason. When X = halogen, the σ-hole is further enlarged and its enlargement increases from the heavier halogen atom to the lighter halogen atom. As expected, the stronger electron-withdrawing groups CN and NO_2 lead to the much larger σ-hole.

3.2. Structures and interaction energies

Fig. S1 of ESI† shows the MP2/aug-cc-pVDZ optimized structures of all binary complexes. First, let's study the carbon-bonded complexes formed by CH_3X. Since there is no σ-hole in CH_3Me and CH_4, the corresponding carbon-bonded complex is not obtained. In general, the N–N–T angle is arranged linearly. However, there is no such linear arrangement in the carbon-bonded complexes. The nonlinear arrangement of some C-containing complexes such as DABCO–CH_3NH_2 can partly attributed to its weak nature and thus it belongs to a van der Waals interaction without directionality, while more unexpected structures are mainly caused by the repulsion between the H atoms in both molecules.

The corresponding binding distances of all complexes are listed in Table 2. For C-bond complexes, the binding distance is shorter than the sum of the corresponding atomic van der Waals radii ($R_{C\cdots N}$ = 3.2 Å), except for CH_3NH_2 of 3.291 Å. In spite of Si and Ge with bigger atomic radii, the respective binding distance is shorter than that of C-bond analogue, and their binding distances are 2.1–2.7 Å and 2.2–2.8 Å, respectively. The relationship between the binding distance and the substituent is worth considering. In most cases, if the substituent causes a bigger σ-hole, the corresponding separation decreases. Interestingly, some exceptions are found. The methyl group elongates the Si···N distance but shortens the Ge···N distance, which is inconsistent with the σ-hole of the Ge atom. For X = halogen, with the increase of X atomic mass, the C···N distance prolongates, while the Si···N and Ge···N distances reduce, inconsistent with the change of the σ-hole on the Si/Ge atom. Although the NO_2 substitution leads to the larger σ-hole than does the F atom, the C···N distance in the CH_3NO_2 complex is longer than that in the CH_3F counterpart.

Upon complexation, the T–X bond is elongated and its elongation is generally related to the strength of tetrel bond (Table S1†). Accompanied with the bond elongation, this bond stretch vibration displays a red shift and this red shift in most complexes is big enough to be observed with experiments.

The interaction energies of all complexes are listed in Table 3. Firstly, we focus on the tetrel bonding strength with different tetrel atoms. Regardless of the X substituent, the interaction energy sequentially increases from CH_3X to GeH_3X to SiH_3X. Generally, the bigger σ-hole on the tetrel atom engages in the

Table 1 The most positive MEP (V_{max}, kcal mol^{-1}) on the σ-hole along the T–R bond in TH_3X

T = C	V_{max}	T = Si	V_{max}	T = Ge	V_{max}
X = CH_3	−2.2	X = CH_3	16.0	X = CH_3	15.7
X = H	−2.1	X = H	22.1	X = H	21.0
X = NH_2	4.1	X = NH_2	22.5	X = NH_2	25.5
X = OH	12.0	X = OH	32.1	X = OH	36.8
X = I	16.3	X = I	38.5	X = I	41.0
X = Br	19.3	X = Br	40.7	X = Br	44.3
X = Cl	20.3	X = Cl	41.7	X = Cl	45.9
X = F	24.1	X = F	45.0	X = F	50.8
X = CN	26.5	X = CN	47.1	X = CN	48.1
X = NO_2	34.9	X = NO_2	61.8	X = NO_2	63.1

Table 2 Binding distance (*R*, Å) in the TH_3X complexes

T = C	*R*	T = Si	*R*	T = Ge	*R*
X = CH_3	—	X = CH_3	2.674	X = CH_3	2.773
X = H	—	X = H	2.657	X = H	2.787
X = NH_2	3.291	X = NH_2	2.423	X = NH_2	2.550
X = OH	3.147	X = OH	2.304	X = OH	2.417
X = I	3.073	X = I	2.179	X = I	2.313
X = Br	3.036	X = Br	2.189	X = Br	2.314
X = Cl	3.058	X = Cl	2.200	X = Cl	2.317
X = F	3.013	X = F	2.222	X = F	2.325
X = CN	3.163	X = CN	2.247	X = CN	2.404
X = NO_2	3.029	X = NO_2	2.122	X = NO_2	2.241

Table 3 Interaction energy (ΔE, kcal mol^{-1}) corrected for BSSE and ZPE in the TH_3X complexes

T = C	ΔE	T = Si	ΔE	T = Ge	ΔE
X = CH_3	—	X = CH_3	−3.7	X = CH_3	−2.7
X = H	—	X = H	−3.7	X = H	−2.7
X = NH_2	−0.9	X = NH_2	−7.2	X = NH_2	−5.5
X = OH	−1.2	X = OH	−11.2	X = OH	−9.1
X = I	−1.7	X = I	−18.4	X = I	−13.7
X = Br	−1.8	X = Br	−18.1	X = Br	−13.9
X = Cl	−2.0	X = Cl	−17.5	X = Cl	−13.9
X = F	−2.0	X = F	−16.4	X = F	−13.7
X = CN	−2.2	X = CN	−14.9	X = CN	−10.4
X = NO_2	−2.7	X = NO_2	−25.0	X = NO_2	−18.9

stronger tetrel bond. However, for the N electron donor in DABCO, the smaller σ-hole on the Si atom forms a stronger tetrel bond than the σ-hole on the Ge atom. Such abnormal result was also reported in the σ-hole tetrel-bonded complexes with NHC,[33] H_3ZO (Z = N, P, As),[65] formamidine[41] as the strong electron donors. The moderate base such as NH_3 usually participates in a stronger tetrel bond with GeH_3X relative to SiH_3X, while an opposite result is obtained when X is 6-*O*-fulvene.[34] This abnormality is partially ascribed to the fact that the silicon atom is more easily polarized than the Ge atom when it binds with a strong Lewis base.

Table S2† lists deformation energy of the complexes. The deformation energy is defined as the energy difference between the isolated molecules and the molecules within the geometry of the complex. This deformation energy is very small (∼0.5 kcal mol^{-1}) in the CH_3X complexes, indicating that both molecules exhibit small distortion. The difference in the deformation energy between the SiH_3X and GeH_3X complexes ranges from 0.5 to 3.1 kcal mol^{-1}. The tetrel bond in the CH_3X complex is much weaker than that in the SiH_3X and GeH_3X complexes.

Then we analyze the effect of the X substituent on the strength of tetrel bond. The methyl group in the tetrel donor weakens the tetrel bond, and this weakening effect is very slight. The role of methyl groups has been explored in different types of interactions such as OH···O hydrogen bond[66] and halogen bond.[67] Generally, the methyl group in both electron donors and acceptors plays an enhancing role in hydrogen bonds. However, the methyl group in the electron acceptor has a weakening effect on the strength of tetrel bond. For –NH_2 and –OH groups, both of them enhance the tetrel bond due to their electron-withdrawing character, and this enhancing effect is larger for the –OH group with an increase of more than 200% in the interaction energy. For the halogen substitution, its effect depends on the nature of the tetrel atom. In the C-bond complex, the tetrel bond is stronger in sequence of I < Br < Cl < F, consistent with the σ-hole at the C–X bond end. In the Si-bond complex, an opposite trend is found. In the Ge-bond complex, the halogen substitution has little effect on the strength of tetrel bond. This shows that the strength of tetrel bond is not only affected by electrostatic interaction but also related to other factors. Although –CN group has the stronger electron-withdrawing ability than –F substitution, the former results in a weaker tetrel bond than the latter in the Si and Ge complexes, inconsistent with the magnitude of the σ-hole. The different in the interaction energy between the TH_3CN and TH_3F complexes varies from 1.5 kcal mol^{-1} for SiH_3X to 3.3 kcal mol^{-1} for GeH_3X. As expected, NO_2 is the strongest electron-withdrawing group and results in the largest o-hole, thus the interaction energy is largest in the TH_3NO_2 complex.

In all, the strength of tetrel bond can be adjusted with the substituent in the tetrel donor. In general, the methyl group weakens the tetrel bond and the other groups strengthen the tetrel bond. Moreover, the influence of substituent is also related to the nature of the tetrel atom. For example, the halogen atom has a different effect on the strength of tetrel bond when the tetrel donor is varied. In addition, the X substituent has a prominent effect on the strength of tetrel bond. For instance, the –NO_2 group increases the interaction energy from −3.7 kcal mol^{-1} in the SiH_4 complex to −25.0 kcal mol^{-1} in the SiH_3NO_2 complex, increased by more than four times. Therefore, the substituent is feasible method for regulating the strength of tetrel bond.

It is interesting to compare different types of interactions involving DABCO. The interaction energy corrected for BSSE was calculated at the MP2/aug-cc-pVTZ level to be respectively −14.6, −19.6, and −26.1 kcal mol^{-1} in the SiH_3F complexes with formamidine,[41] H_3NO,[64] and NHC,[33] which are often taken as stronger electron donors. The interaction energy corrected for BSSE and ZPE at the MP2/aug-cc-pVDZ level is −16.4 kcal mol^{-1} in DABCO–SiH_3F. Thus DABCO is also a good electron donor in the tetrel bond. At the CCSD(T)/CBS level, the interaction energy was in a range of 9–26.5 kcal mol^{-1} in the halogen-bonded complexes of DABCO with dihalogen.[57] Thus we think that DABCO has a comparable affinity to the halogen and tetrel atoms.

In most hydrogen bonds, both binding distance and interaction energy display a linear relationship. Fig. S2† shows the relationship between the binding distance and the interaction energy in the tetrel-bonded complexes. No relationship is found for them in the CH_3X complex, while a quadratic relationship is present between them in the SiH_3X and GeH_3X complexes, with a correlation coefficient of 0.993 and 0.996, respectively.

3.3. AIM analyses

AIM analysis can provide some useful information for the existence of noncovalent interactions as well as the strength and nature of each interaction. Fig. 3 shows the AIM diagram obtained by AIM2000 software. We only plotted the AIM diagram of DABCO···GeH_3NO_2 since others are similar. Obviously, there is a Ge···N BCP, providing an evidence for the existence of a tetrel bond.

Table 4 presents the topological parameters including the electron density (ρ), its Laplacian ($\nabla^2\rho$), and total energy density (H) at the intermolecular BCP in the TH_3X complexes. The electron density at the C···N BCP is small, less than 0.011 au, and its change is irregular. The electron densities at the Si···N and Ge···N BCPs are comparable each other and they exhibit an

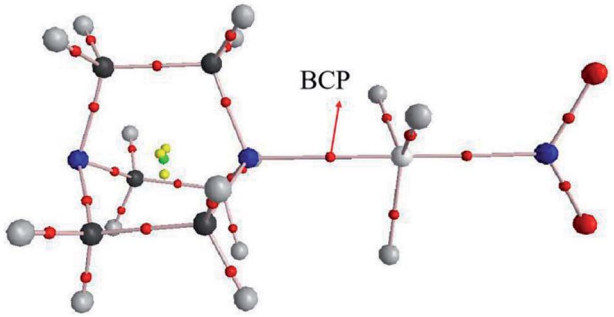

Fig. 3 AIM diagram of DABCO···GeH_3NO_2.

exponential relationship with the binding distance as shown in Fig. S3.† The corresponding correlation coefficients are 0.994 and 0.988. Both Laplacian and energy density at the C···N BCP are positive, confirming the weak interaction and a closed-shell interaction in the CH_3X complex. However, in the SiH_3X and GeH_3X complexes, the energy density becomes negative though its Laplacian is still positive. This indicates that the Si···N and Ge···N tetrel bond has a partially covalent character.[68–77] The stronger Si···N interaction has the more negative energy density than the Ge···N analogue.

3.4. NBO analyses

The orbital interaction and charge transfer were analyzed for all complexes. For the C-bond complexes, there is only one type of orbital interaction: Lp(N) → σ*(C–X), where Lp(N) denotes the lone pair orbital of N atom and σ*(C–X) is the anti-bonding orbital of C–X bond. However, for the Si- and Ge-bond complexes, there are two types of orbital interactions. In addition to Lp(N) → σ*(T–X), there is also an orbital interaction of Lp(N) → σ*(T–H). The strength of these orbital interactions is estimated with second-order perturbation energies in Table 5, where $E_1^{(2)}$ is for Lp(N) → σ*(T–X) and $E_2^{(2)}$ for the sum of three Lp(N) → σ*(T–H) orbital interactions. From the table we can see that for the C-bond system, $E_1^{(2)}$ is very small, about 0.5–2.0 kcal mol^{-1}, consistent with the weak interaction in the C-bond complex. The Si- and Ge-bond complexes have large $E^{(1)}$ values, and $E_1^{(2)}$ is larger than $E_2^{(2)}$. Thus the Lp(N) → σ*(T–X) orbital interaction is dominant in the tetrel bond. Regardless of the orbital interaction, the value of $E^{(2)}$ in the Si-bond system is greater than that of the Ge-bond system, which has the same order as the interaction energy. For the halogen substitution, both types of orbital interactions show an increasing tendency from F to I, particularly for the Lp(N) → σ*(T–X) orbital interaction. Therefore, some abnormal results in the tetrel bond can be partly explained with the orbital interactions.

The formation of tetrel-bonded complexes leads to charge transfer from the Lewis base to the acid. So the amount of charge transfer can to a certain extent reflect the strength of tetrel bond. For the C-bond complexes, the value of charge transfer is very small, only between 0.002–0.005*e*, corresponding to the weak interaction. For the Si- and Ge-bond complexes, the amount of charge transfer is relatively large, and the Si complex has the greater charge transfer than the Ge analogue. We also made a graph of the relationship between charge transfer and interaction energy, as shown in Fig. S4.† No relationship is found in the C-bond complex, while a linear relationship is present between them for the Si and Ge complexes. The correlation coefficients are 0.973 and 0.983 for the Si and Ge systems, respectively. Therefore, charge transfer is of great important in the formation of Si- and Ge-bond complexes.

3.5. Energy decomposition analyses

To have a deep insight into the origin of the tetrel bond, the interaction energies of all complexes were decomposed into electrostatic (E^{ele}), exchange (E^{ex}), repulsion (E^{rep}), polarisation (E^{pol}), and dispersion energies (E^{disp}). Both E^{rep} and E^{ex} are partly cancelled each other, so we only focused on three attractive terms (E^{ele}, E^{pol}, and E^{disp}). For easy comparison, these terms were plotted in Fig. 4. For the C-bond complex, E^{pol} is smallest; E^{disp} dominates over E^{ele} when the substituent is NH_2, OH and I, while E^{ele} exceeds E^{disp} in the case of the remaining substituents. These quantities have a similar variation in the Si- and Ge-bond complexes. E^{ele} is greater than E^{pol} and E^{disp}, confirming the electrostatic nature of tetrel bonding. For the different substituents, both E^{ele} and E^{pol} change uniformly, and E^{disp} is little changed. For the halogen substitution, both E^{ele} and E^{pol} increase from F to I. Fig. S5† shows the relationship between the total interaction energy and E^{ele}/E^{pol} in the Si- and

Table 4 Electron density (*ρ*, a.u.), its Laplacian ($\nabla^2\rho$, a.u.), and total energy density (*H*, a.u.) at the intermolecular BCP in the TH_3X complexes

	T = C			T = Si			T = Ge		
	ρ	$\nabla^2\rho$	*H*	*ρ*	$\nabla^2\rho$	*H*	*ρ*	$\nabla^2\rho$	*H*
X = CH_3	—	—	—	0.024	0.042	−0.003	0.022	0.052	−0.001
X = H	—	—	—	0.025	0.041	−0.004	0.024	0.050	−0.002
X = NH_2	0.005	0.023	0.001	0.035	0.047	−0.010	0.035	0.047	−0.010
X = OH	0.008	0.029	0.001	0.042	0.063	−0.015	0.041	0.100	−0.007
X = I	0.009	0.034	0.002	0.048	0.137	−0.014	0.048	0.136	−0.010
X = Br	0.010	0.035	0.002	0.050	0.102	−0.018	0.051	0.119	−0.012
X = Cl	0.011	0.033	0.002	0.050	0.096	−0.018	0.050	0.119	−0.012
X = F	0.009	0.037	0.002	0.046	0.090	−0.004	0.049	0.119	−0.011
X = CN	0.008	0.029	0.001	0.046	0.072	−0.017	0.043	0.100	−0.008
X = NO_2	0.010	0.034	0.002	0.056	0.144	−0.019	0.059	0.137	−0.016

Table 5 Charge transfer (CT, *e*) and second-order perturbation energies ($E^{(2)}$, kcal mol^{-1}) in the TH_3X complexes[a]

	CT			$E_1^{(2)}$			$E_2^{(2)}$		
	T = C	T = Si	T = Ge	T = C	T = Si	T = Ge	T = C	T = Si	T = Ge
X = CH_3	—	0.038	0.030	—	8.0	7.3	—	2.7	2.3
X = H	—	0.037	0.027	—	7.5	6.3	—	2.6	2.2
X = NH_2	0.003	0.064	0.051	0.5	14.5	12.7	—	5.7	4.5
X = OH	0.003	0.083	0.071	1.1	19.1	17.1	—	7.8	6.5
X = I	0.004	0.121	0.100	1.6	31.0	27.5	—	10.3	8.4
X = Br	0.005	0.118	0.101	1.8	28.7	26.2	—	10.1	8.3
X = Cl	0.005	0.113	0.099	1.7	27.1	24.8	—	9.9	8.2
X = F	0.005	0.098	0.089	2.1	23.0	21.2	—	9.0	7.9
X = CN	0.002	0.105	0.081	0.8	22.3	18.1	—	9.1	6.7
X = NO_2	0.005	0.140	0.122	2.0	33.6	30.9	—	12.0	10.3

[a] $E_1^{(2)}$ and $E_2^{(2)}$ correspond to the Lp(N) → σ*(T–R) and Lp(N) → σ*(T–H) orbital interactions, respectively.

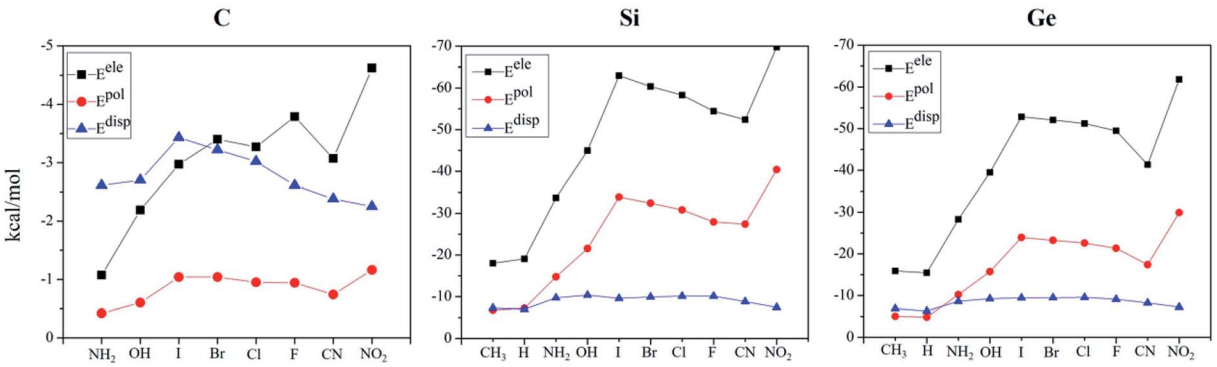

Fig. 4 Variation of three attractive terms (E^{ele}, E^{pol}, and E^{disp}) on the substituents.

Ge-bond complexes. Obviously, a good linear relationship is present between them. Thus the strength of tetrel bond in the TH_3X (T = Si and Ge) complex is jointly controlled by electrostatic and polarization interactions.

4. Conclusions

The complexes of DABCO···TH_3X (T = C, Si, and Ge) have been studied with theoretical methods in view of the geometrics, energetics, charge transfer, orbital interactions, and AIM parameters. The main conclusions are summarized as:

(1) The interaction energy of DABCO···TH_3X is comparable with that of stronger Lewis bases such as NHC, formamidine, and H_3NO, indicating that DABCO is also a good electron donor in the tetrel bond.

(2) The tetrel bond strengthens in order of C < Ge < Si, inconsistent with the magnitude of σ-hole on the tetrel atom. It is primarily attributed to the stronger orbital interaction in the SiH_3X systems.

(3) The methyl group in the tetrel donor weakens the tetrel bond, while the other substituents enhance it. The substituents have a small effect on the strength of tetrel bond in the C-bond complex but a larger effect in the Si- and Ge-bond complexes. For the halogen substitution from F to I, the tetrel bond weakens a little in the C-bond complex, strengthens in the Si-bond complex, and is almost not changed in the Ge-bond complex. Thus the substitution effect on the strength of tetrel bond is also related to the nature of the tetrel atom. The strongest electron-withdrawing group NO_2 results in the strongest tetrel bond.

(5) The tetrel bond is a closed-shell interaction in the C-bond complex but a partially covalent interaction in the Si- and Ge-bond complexes.

(6) Three attractive terms (E^{ele}, E^{pol}, and E^{disp}) are small and show an irregular change in the C-bond complex but a similar variation is found in the Si- and Ge-bond complexes. In the stronger tetrel bond, both E^{ele} and E^{pol} display a linear relationship with the interaction energy although the former has a larger contribution.

Conflicts of interest

There are no conflicts to declare.

Acknowledgements

This work was supported by the National Natural Science Foundation of China (21573188) and Open Subject of Faculty of

Chemistry of QingDao University of Science and Technology (QUSTHX201807).

References

1 G. Mahmoudi, A. Bauzá and A. Frontera, *Dalton Trans.*, 2016, **45**, 4965–4969.
2 G. Mahmoudi, A. Bauzá, M. Amini, E. Molins, J. T. Mague and A. Frontera, *Dalton Trans.*, 2016, **45**, 10708–10716.
3 M. S. Gargari, V. Stilinović, A. Bauzá, A. Frontera, P. McArdle, D. V. Derveer, S. W. Ng and G. Mahmoudi, *Chem.–Eur. J.*, 2016, **21**, 17951–17958.
4 S. J. Grabowski, *Phys. Chem. Chem. Phys.*, 2014, **16**, 1824–1834.
5 M. X. Liu, J. B. Cheng, H. B. Li and Q. Z. Li, *J. Chem. Phys.*, 2016, **145**, 224310.
6 J. Mikosch, S. Trippel, C. Eichhorn, R. Otto, U. Lourderaj, J. X. Zhang, W. L. Hase, M. Weidemüller and R. Wester, *Science*, 2008, **319**, 183–186.
7 G. R. Desiraju, *J. Am. Chem. Soc.*, 2001, **123**, 191–192.
8 X. García-LLinás, A. Bauzá, S. K. Seth and A. Frontera, *J. Phys. Chem. A*, 2017, **121**, 5371–5376.
9 V. R. Mundlapati, D. K. Sahoo, S. Bhaumik, S. Jena, A. Chandrakar and H. S. Biswal, *Angew. Chem., Int. Ed.*, 2018, **57**, 16496–16500.
10 P. Politzer, J. S. Murray and T. Clark, *Phys. Chem. Chem. Phys.*, 2013, **15**, 11178–11189.
11 J. S. Murray, P. Lane and P. Politzer, *J. Mol. Model.*, 2009, **15**, 723–729.
12 A. Bauzá, T. J. Mooibroek and A. Frontera, *ChemPhysChem*, 2015, **16**, 2496–2517.
13 T. Clark, M. Hennemann, J. S. Murray and P. Politzer, *J. Mol. Model.*, 2007, **13**, 291–296.
14 J. S. Murray, P. Lane, T. Clark, K. E. Riley and P. Politzer, *J. Mol. Model.*, 2012, **18**, 541–548.
15 G. R. Desiraju, P. S. Ho, L. Kloo, A. C. Legon, R. Marquardt, P. Metrangolo, P. Politzer, G. Resnati and K. Rissanen, *Pure Appl. Chem.*, 2013, **85**, 1711–1713.
16 W. Z. Wang, B. M. Ji and Y. Zhang, *J. Phys. Chem. A*, 2009, **113**, 8132–8135.
17 S. Zahn, R. Frank, E. Hey-Hawkins and B. Kirchner, *Chem.–Eur. J.*, 2011, **17**, 6034–6038.
18 A. Bauzá, T. J. Mooibroek and A. Frontera, *Angew. Chem., Int. Ed.*, 2013, **52**, 12317–12321.
19 S. Scheiner, *J. Phys. Chem. A*, 2015, **119**, 9189–9199.
20 K. J. Donald and M. Tawfik, *J. Phys. Chem. A*, 2013, **117**, 14176–14183.
21 A. Bundhun, P. Ramasami, J. S. Murray and P. Politzer, *J. Mol. Model.*, 2013, **19**, 2739–2746.
22 S. A. C. Mcdowell and J. A. Joseph, *Phys. Chem. Chem. Phys.*, 2014, **16**, 10854–10860.
23 Q. Z. Li, X. Guo, X. Yang, W. Z. Li, J. B. Cheng and H. B. Li, *Phys. Chem. Chem. Phys.*, 2014, **16**, 11617–11625.
24 Q. Z. Li, H. Y. Zhuo, H. B. Li, Z. B. Liu, W. Z. Li and J. B. Cheng, *J. Phys. Chem. A*, 2015, **119**, 2217–2224.
25 M. D. Esrafili and F. Mohammadiansabet, *J. Mol. Model.*, 2015, **21**, 1–8.
26 D. Mani and E. Arunan, *J. Phys. Chem. A*, 2014, **118**, 10081–10089.
27 N. W. Mitzel and U. Losehand, *Angew. Chem., Int. Ed.*, 1997, **36**, 2807–2809.
28 N. W. Mitzel, A. J. Blake and D. W. H. Rankin, *J. Am. Chem. Soc.*, 1997, **119**, 4143–4148.
29 S. B. Choi, B. K. Kim, P. Boudjouk and D. G. Grier, *J. Am. Chem. Soc.*, 2001, **123**, 8117–8118.
30 M. D. Esrafili, H. Behzadi and N. L. Hadipour, *Chem. Phys.*, 2008, **348**, 175–180.
31 I. Alkorta, F. Blanco and J. Elguero, *Struct. Chem.*, 2009, **20**, 63–71.
32 M. D. Esrafili and S. Shahabivand, *Struct. Chem.*, 2014, **25**, 403–408.
33 M. X. Liu, Q. Z. Li, W. Z. Li and J. B. Cheng, *Struct. Chem.*, 2017, **28**, 823–831.
34 M. C. Hou, S. B. Yang, Q. Z. Li, J. B. Cheng, H. B. Li and S. F. Liu, *Molecules*, 2019, **24**, 10.
35 K. Nakamura, T. Hatakeyama and H. Hatakeyama, *Polym. J.*, 1983, **15**, 361–366.
36 M. Yoosefian, H. Raissi, E. S. Nadim, F. Farzad, M. Fazli, E. Karimzade and A. Nowroozi, *Int. J. Quantum Chem.*, 2011, **111**, 3505–3516.
37 N. Kim, H. Lee, K. Choi, J. A. Yu, C. J. Yoon, J. Park and Y. S. Choi, *J. Phys. Chem. A*, 2000, **104**, 5572–5578.
38 M. Solimannejad, M. Malekani and I. Alkorta, *J. Phys. Chem. A*, 2013, **117**, 5551–5557.
39 A. C. C. Carlsson, K. Mehmeti, M. Uhrbom, A. Karim, M. Bedin, R. Puttreddy, R. Kleinmaier, A. A. Neverov, B. Nekoueishahraki, J. Gräfenstein, K. Rissanen and M. Erdélyi, *J. Am. Chem. Soc.*, 2016, **138**, 9853–9863.
40 A. Bauzá, D. Quiñonero, A. Frontera and P. M. Deyà, *Phys. Chem. Chem. Phys.*, 2011, **13**, 20371–20379.
41 H. L. Xu, J. B. Cheng, X. F. Yu and Q. Z. Li, *ChemistrySelect*, 2018, **3**, 2842–2849.
42 S. Scheiner, *J. Phys. Chem. A*, 2017, **121**, 5561–5568.
43 W. B. Dong, Q. Z. Li and S. Scheiner, *Molecules*, 2018, **23**, 1681.
44 M. X. Liu, Q. Z. Li and S. Scheiner, *Phys. Chem. Chem. Phys.*, 2017, **19**, 5550–5559.
45 S. Pan, D. Moreno, S. Ghosh, P. K. Chattaraj and G. Merino, *J. Comput. Chem.*, 2016, **37**, 226–236.
46 M. Ghara, S. Pan, A. Kumar, G. Merino and P. K. Chattaraj, *J. Comput. Chem.*, 2016, **37**, 2202–2211.
47 S. Pan, D. Moreno, G. Merino and P. K. Chattaraj, *ChemPhysChem*, 2014, **15**, 3554–3564.
48 F. S. Fernandes, M. T. Rodrigues Jr, L. A. Zeoly, C. Conti, C. F. F. Angolini, M. N. Eberlin and F. Coelho, *J. Org. Chem.*, 2018, **83**, 15118–15127.
49 P. T. Kaye and R. S. Robinson, *Synth. Commun.*, 1996, **26**, 2085–2097.
50 S. H. Zhao, D. Wang, M. Wang, J. Tang and L. W. Zhang, *Chin. J. Org. Chem.*, 2015, **35**, 865–874.
51 R. Saravanakumar, B. Varghese and S. Sankararaman, *J. Mol. Struct.*, 2014, **1076**, 280–284.

52 M. Shiga, S. Kawaguchi, M. Fujibayashi, S. Nishihara, K. Inoue, T. Akutagawa, S. Noro, T. Nakamura and R. Tsunashima, *Dalton Trans.*, 2018, **47**, 7656–7662.
53 S. Dordonne, B. Crousse, D. Bonnet-Delpon and J. Legros, *Chem. Commun.*, 2011, **47**, 5855–5857.
54 A. Peuronen, A. Valkonen, M. Kortelainen, K. Rissanen and M. Lahtinen, *Cryst. Growth Des.*, 2012, **12**, 4157–4169.
55 Y. L. Ma, H. Ke, A. Valkonen, K. Rissanen and W. Jiang, *Angew. Chem., Int. Ed.*, 2017, **57**, 709–713.
56 T. Asaji, K. Shido and H. Fujimori, *J. Mol. Struct.*, 2018, **1169**, 81–84.
57 P. Deepa, R. Sedlak and P. Hobza, *Phys. Chem. Chem. Phys.*, 2014, **16**, 6679–6686.
58 M. J. Frisch, H. B. Schlegel, G. E. Scuseria, M. A. Robb,J. R. Cheeseman, G. Scalmani, V. Barone, B. Mennucci, G. A. Petersson, H. Nakatsuji, M. Caricato, X. Li, H. P. Hratchian, A. F. Izmaylov, J. Bloino, G. Zheng, J. L. Sonnenberg, M. Hada, M. Ehara, K. Toyota, R. Fukuda, J. Hasegawa, M. Ishida, T. Nakajima, Y. Honda, O. Kitao, H. Nakai, T. Vreven, J. A. Montgomery Jr, J. E. Peralta, F. Ogliaro, M. Bearpark, J. J. Heyd, E. Brothers, K. N. Kudin, V. N. Staroverov, R. Kobayashi, J. Normand, K. Raghavachari, A. Rendell, J. C. Burant, S. S. Iyengar, J. Tomasi, M. Cossi, N. Rega, J. M. Millam, M. Klene, J. E. Knox, J. B. Cross, V. Bakken, C. Adamo, J. Jaramillo, R. Gomperts, R. E. Stratmann, O. Yazyev, A. J. Austin, R. Cammi, C. Pomelli, J. W. Ochterski, R. L. Martin, K. Morokuma, V. G. Zakrzewski, G. A. Voth, P. Salvador, J. J. Dannenberg, S. Dapprich, A. D. Daniels, O. Farkas, J. B. Foresman, J. V. Ortiz, J. Cioslowski and D. J. Fox, *Gaussian 09, revision A02*, Gaussian Inc., Wallingford, 2009.
59 S. B. Boys and F. Bernardi, *Mol. Phys.*, 1970, **19**, 553–566.
60 F. A. Bulat, A. Toro-Labbé, T. Brinck, J. S. Murray and P. Politzer, *J. Mol. Model.*, 2010, **16**, 1679–1691.
61 R. F. W. Bader, *AIM2000 program, version 2.0*, McMasterUniversity, Hamilton, Canada, 2000.
62 A. E. Reed, L. A. Curtiss and F. A. Weinhold, *Chem. Rev.*, 1988, **88**, 899–926.
63 M. W. Schmidt, K. K. Baldridge, J. A. Boatz, S. T. Elbert, M. S. Gordon, J. H. Jensen, S. Koseki, N. Matsunaga, K. A. Nguyen, S. J. Su, T. L. Windus, M. Dupuis and J. A. Montgomery, *J. Comput. Chem.*, 1993, **14**, 1347–1363.
64 P. F. Su and H. Li, *J. Chem. Phys.*, 2009, **13**, 014102.
65 H. L. Xu, J. B. Cheng, H. B. Li, X. Yang and Q. Z. Li, *Int. J. Quantum Chem.*, 2018, **118**, e25660.
66 Q. Z. Li, N. N. Wang and Z. W. Yu, *J. Mol. Struct.: THEOCHEM*, 2008, **862**, 74–79.
67 Q. Z. Li, B. Jing, Z. B. Liu, W. Z. Li, J. B. Cheng, B. Z. Gong and J. Z. Sun, *J. Chem. Phys.*, 2010, **133**, 114303.
68 W. D. Arnold and E. Oldfield, *J. Am. Chem. Soc.*, 2000, **122**, 12835–12841.
69 S. Pan, A. Gupta, S. Mandal, D. Moreno, G. Merino and P. K. Chattaraj, *Phys. Chem. Chem. Phys.*, 2015, **17**, 972–982.
70 G. Jana, R. Saha, S. Pan, A. Kumar, G. Merino and P. K. Chattaraj, *ChemistrySelect*, 2016, **1**, 5842–5849.
71 M. Ghara, S. Pan, J. Deb, A. Kumar, U. Sarkar and P. K. Chattaraj, *J. Chem. Sci.*, 2016, **128**, 1537–1548.
72 S. Pan, R. Saha, A. Kumar, A. Gupta, G. Merino and P. K. Chattaraj, *Int. J. Quantum Chem.*, 2016, **116**, 1016–1024.
73 S. Pan, R. Saha, S. Mandal and P. K. Chattaraj, *Phys. Chem. Chem. Phys.*, 2016, **18**, 11661–11676.
74 G. Jana, S. Pan, G. Merino and P. K. Chattaraj, *J. Phys. Chem. A*, 2017, **121**, 6491–6499.
75 G. Jana, S. Pan and P. K. Chattaraj, *J. Phys. Chem. A*, 2017, **121**, 3803–3817.
76 G. Jana, S. Pan, G. Merino and P. K. Chattaraj, *J. Phys. Chem. A*, 2018, **122**, 7391–7401.
77 G. Jana, S. Pan, E. Osorio, L. Zhao, G. Merino and P. K. Chattaraj, *Phys. Chem. Chem. Phys.*, 2018, **20**, 18491–18502.

